

# Boundary mixing in a stratified fluid

By G. N. IVEY

Canada Centre for Inland Waters, P.O. Box 5050, Burlington, Ontario L7R 4A6

AND G. M. CORCOS

Department of Mechanical Engineering, University of California, Berkeley, CA94720

(Received 13 April 1981 and in revised form 20 January 1982)

A vertically oscillating grid is used to simulate boundary mixing in the laboratory. The oscillation of the grid creates a turbulent mixing region in its vicinity, and mixing within this region creates a step-like structure in an initial density distribution which varies linearly with depth. If the initial density varies only at the boundary between two homogeneous layers, the same grid turbulence generates additional steps above and below the initial one. The steps, in turn, drive multiple intrusions of mixed fluid away from the boundary and into the non-turbulent interior of the fluid. A compensating return flow carries fluid from the interior into the turbulent mixing region. From the data, the inference is made that the intrusions make a negligible direct contribution to the vertical mass transport. An analytical model of the intrusions, which employs only molecular values of the transport coefficients and also demonstrates negligible vertical mass transport, is consistent with the laboratory observations.

Nevertheless, the data indicate that the fluid eventually reaches a homogeneous density by means of the gradual change of the gradient at a rate which is essentially the same both near the grid and far from it. For an initially uniform density profile this change occurs at all heights simultaneously, and for an initial density step it occurs preferentially near the step. Thus in both cases the interior flow must include slow vertical advection away from the horizontal centre plane. These advective currents can be made part of a consistent dynamic model, the buoyant equivalent of the spin-down in a rotating flow, provided that the net effect of the grid mixing includes a decrease in the local *slope* of the density gradient. This mode of adjustment explains satisfactorily the experimentally observed negligible horizontal density gradients. For the case of an initially uniform density stratification, the shape of the evolving density gradient is not accounted for. In particular, it is not clear why the gradient changes at mid-depth almost simultaneously with variations at top and bottom boundaries.

The vertical mass flux is found to be independent of container length, and it increases with grid frequency of oscillation, amplitude of oscillation and with the mean density gradient.

---

## 1. Introduction

In order to utilize effectively the potential resources of the world's natural water bodies, it is necessary to understand the physical processes which govern advection and mixing and which determine the very properties of these water bodies. Lakes and oceans are commonly stratified in density. In the upper layers, the mixing process has

been the subject of intensive investigation in recent years (see the reviews by Krauss 1977; Sherman, Imberger & Corcos 1978). However, weak flow and slow mixing processes are observed in the hypolimnion, and, although important, the dynamics of this region are poorly understood.

This lack of understanding is, to a large extent, attributable to the scarcity of observations of flows and mixing events in this region. A number of mechanisms have been proposed to explain the weak vertical mixing in the hypolimnion: double-diffusive phenomena, mixing associated with temporary and infrequent distortion of the pycnocline (as a result of storms for example), interactions and instabilities involving internal waves, and mixing at the boundaries. Since double-diffusive effects are confined to fluids whose density is determined by a two-component system, it cannot be invoked as a general explanation of mixing in fresh water. There have been no observations to date on the influence of storms on hypolimnetic mixing, and the role of this mechanism remains purely speculative. Internal waves can break while propagating through continuously stratified fluids and result in weak local mixing. Recent estimates by Garrett (1979*a*), however, suggest that this mechanism does not fully explain the observed mixing rates, and further work is required to refine these estimates. There remains then the possibility that mixing adjacent to solid boundaries is responsible for an important fraction of the apparent vertical mixing in the entire lake or ocean basin – a suggestion first advanced by Munk (1966).

In the oceans, mesoscale eddies may drive a mean flow over the hydraulically rough bottom topography and create localized turbulent mixing. Armi & Millard (1976) and Armi (1978, 1979) have shown that this boundary-mixed water is found in the interior of the ocean basins. In lakes there is also the possibility of an oscillatory external flow over the rough bottom due to seiching action. In lakes of small and medium size, Fischer *et al.* (1979) suggest that boundary mixing driven by seiching motion may even be the dominant cause of hypolimnetic mixing. But the mechanism by which boundary mixing is communicated to the interior is not clear. If fluid mixed near the boundaries is found in the interior, it must be advected there, probably along isopycnic surfaces. Does the advection itself enhance the vertical transport? What is the nature of the turbulence in the vicinity of the boundary, and how is it affected by the local density gradient?

It occurred to us that at least some of these questions could be studied in a small-scale laboratory experiment using a stratified fluid. Jörg Imberger (personal communication) had also been interested in such an experiment for some time.

## 2. Experiment

When buoyancy seriously affects the flow, it is seldom possible to reach sufficiently high Reynolds numbers to create turbulence naturally as the result of shear. Consequently one is forced to generate turbulence mechanically, e.g. by oscillating a grid. It follows that the quantitative results depend on parameters which are not readily identified under natural circumstances. This course was reluctantly followed in the present experiment, which had the compensating merit of simplicity. A rough vertical plane was oscillated vertically at one end of a rectangular tank. The water in the tank was stratified by a salt solution. Initially, the vertical stratification was either linear or consisted of a single step. The length and depth of the tank, the frequency and

amplitude of grid oscillation, and the strength of the density stratification were all varied. The flow was observed with a simple shadowgraph and with dye. The density was measured with a fast-response travelling concentration probe.

The experiments were conducted in a glass-sided metal-framed tank with dimensions 1.83 m in length, 0.305 m in width and 0.91 m in depth. The rough plate was mounted vertically, flush with the end wall, located by a system of four small adjustable brass guides and roller bearings, and left free to oscillate vertically. The roughness was created by machining a series of horizontal grooves (1.27 cm square grooves with a 2.54 cm centre line to centre line spacing) in a single sheet of Lucite with dimensions 0.91 m in height, 0.30 m in width, and 2.54 cm in thickness. In operation, the movement of the Lucite grid over the Lucite end wall was water-lubricated and, for the section of grid not immersed in water (usually the top 15 cm), a thin piece of Teflon was glued to the end wall to prevent binding. The grid was oscillated vertically via an eccentric crank and arm linkage. The crank radius was adjustable, but a typical ratio of arm length to crank radius was about 25, which yielded a close approximation to a simple sinusoidal motion.

The density stratification in the tank was established by the addition of sodium chloride. The two-tank method of Fortuin (1960) was used to generate a linear or a two-layer salt-stratified solution as desired.

The principal instrument utilized in this study was a conductivity probe. The probe consisted of a 1 m length of thin-walled stainless steel tubing with an outside diameter of 3.2 mm. Two fine (0.25 mm diameter) platinum wires were mounted 2 mm apart on the end of the tube and trimmed to a length of 3 mm. The probe was mounted in a carriage placed on parallel rails bolted to the top of the tank. The carriage enabled the positioning of the probe at any point in the tank, and the probe was then traversed vertically with the aid of a small electric motor. The vertical position of the probe was recorded with the aid of a helical potentiometer, geared directly to the driving motor. The probe formed part of one arm of an AC Wheatstone bridge circuit which was excited by a 6 V r.m.s. 3 kHz signal.

The outputs from the displacement circuit and the bridge circuit were recorded on the  $x$ - and  $y$ -co-ordinates, respectively, of an  $(x, y)$  flat-bed plotter. The resulting conductivity traces with depth were converted to density versus depth traces by calibration against a range of solutions of known density, and over the duration of one experiment this enabled densities to be computed with an accuracy of 2% of the total density variation. Flow visualization was accomplished by means of both a simple shadowgraph and the use of Rhodamine WT dye.

### 3. Experimental observations

The experimental arrangement enabled the variation of the ambient density stratification, the frequency  $\omega$  of oscillation of the grid, the amplitude  $a$  of oscillation of the grid, the tank length  $L$  and, to a lesser extent, the water depth  $H$ . A summary of the experimental program is given in table 1. In all experiments, the grid Reynolds number defined as  $Re_g = (\omega a)d/\nu$  was of order  $10^3$ , where the appropriate length scale  $d$  was taken as the bar size (1.27 cm).

The results of a typical dye-injection study for an experiment with an initial linear stratification are shown in figures 1 ( $a-d$ ). The sequence depicts the time history of a

Experiment	$\omega$ (rad/s)	$a$ (cm)	$L$ (m)	$H$ (cm)	Initial stratification		$Re_g$ ( $\times 10^{-3}$ )	Duration (min)
					type	$N^2$ (rad <sup>2</sup> /s <sup>2</sup> )		
1	25.1	1.0	1.83	68	linear	0.30	3.18	179
2	25.2	1.0	1.83	55.5	linear	0.35	3.19	181
3	25.1	1.0	1.83	69	two-layer	0.76	3.18	146
4	24.7	1.0	1.83	70	two-layer	8.04	3.12	73
5	25.1	1.0	1.83	70	two-layer	12.60	3.18	169
6	24.6	0.50	1.83	71.5	two-layer	3.09	1.56	219
7	24.7	0.70	1.83	70	two-layer	18.70	2.19	106
8	24.9	1.10	1.83	70	two-layer	7.50	3.46	125
9	18.8	0.70	1.83	71	two-layer	4.07	1.66	196
10	26.0	0.70	1.83	70	two-layer	8.92	2.30	78
11	31.4	0.70	1.83	70	two-layer	8.24	2.78	93
12	33.0	0.70	1.83	71	two-layer	2.74	2.92	71
13	41.7	0.70	1.83	71	two-layer	6.81	3.69	37
14	24.0	0.70	1.83	68	two-layer	2.35	2.13	157
15	39.8	0.70	1.83	70	two-layer	2.55	3.52	104
16	24.9	1.10	0.92	70	two-layer	5.89	3.46	48
17	24.9	1.10	1.25	71	two-layer	6.37	3.46	59
18	24.6	0.52	1.83	54.5	two-layer	6.37	1.62	204
19	43.5	0.70	1.83	70	two-layer	2.94	3.85	44
20	25.1	1.00	1.83	69	two-layer	1.52	3.18	76
21	20.9-44.0	0.52	1.83	68	linear	0.34	1.37-2.89	—
22	26.7-46.3	0.52-1.00	1.83	68	linear	0.34	1.76-3.05	—
23	15.7-35.4	0.68	1.83	68	linear	0.31	1.35-3.04	—
24	15.7-40.6	0.46	1.83	68	linear	0.14	0.91-2.36	—
25	16.8-31.4	0.68	1.83	68	linear	0.14	1.45-2.70	—
26	27.9	0.48	1.83	68	linear	0.15	1.69	37
27	25.3	0.50	1.83	68	linear	0.28	1.60	115
28	24.9	0.50	1.83	71	two-layer	1.81	1.57	109

TABLE 1. Summary of the experimental programme. For the two-layer stratification,  $N^2$  was computed across the interfacial region. Kinematic viscosity  $\nu = 1.004 \times 10^{-6}$  m<sup>2</sup>/s at 20 °C was used in computing  $Re_g$ . Frequencies and amplitudes were varied in discrete intervals over the ranges shown for experiments 21 to 25.

neutrally buoyant dye cloud. The photographs clearly reveal a series of horizontal intrusions which emanated from a grid-bound turbulent mixing region and propagated slowly out into the quiescent interior. The dye streak introduced in figure 1(c) shows the vertically oscillating displacement profile associated with these intrusions. It also indicates that strong flows occurred in two boundary regions near the top and bottom of the water column. Within these regions, the dye cloud spread vertically and horizontally far more rapidly than in the interior. This rapid mixing was probably driven by energetic vortices observed in the two corner regions adjacent to the grid. Such corner vortices have been observed in other grid-stirring experiments (e.g. Hopfinger & Toly 1976).

Conductivity profiles provide further information about the character of this intrusive flow. Figure 2 shows a series of six profiles taken in rapid succession along the centre line of the tank. They show a regular oscillation or step-like structure of density with depth. Furthermore, the oscillations decay with increasing distance from

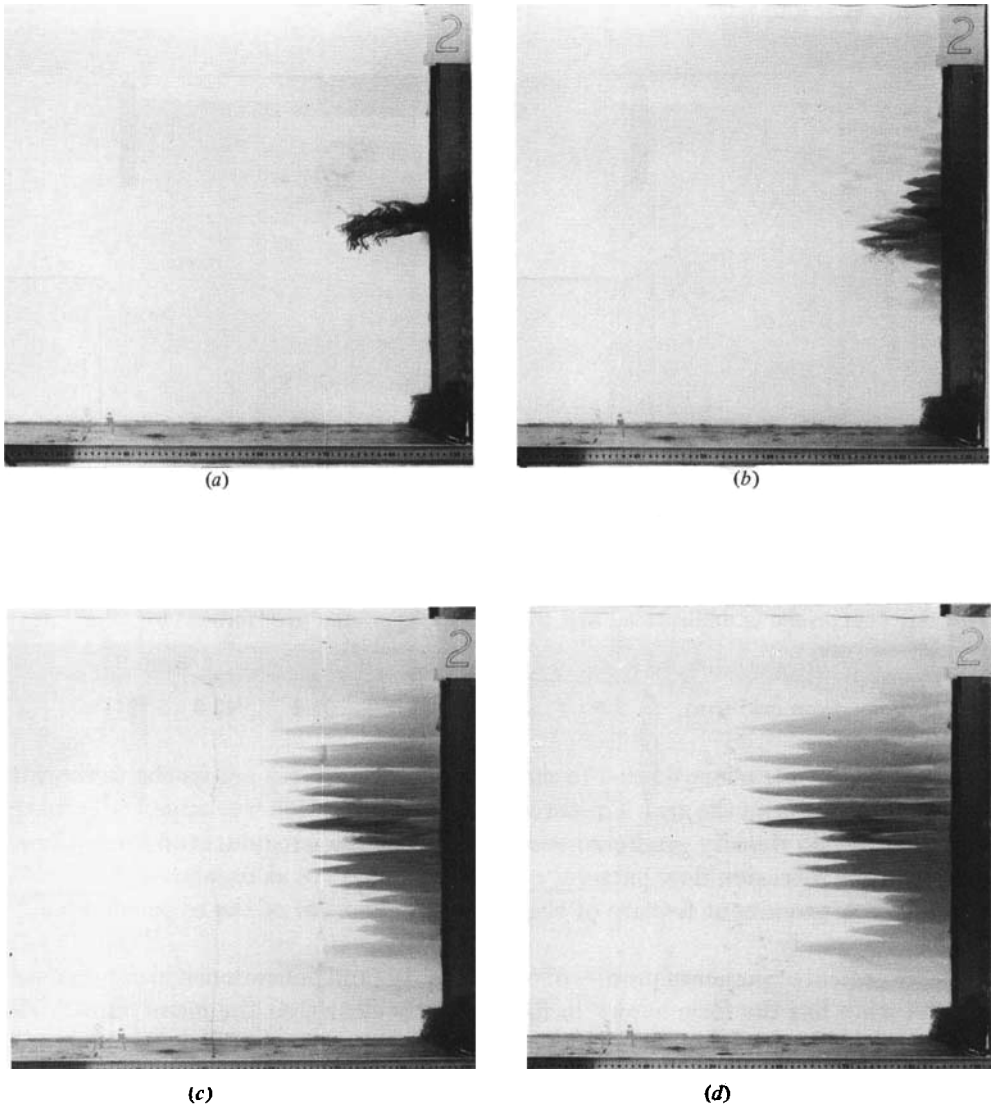


FIGURE 1. Experiment 27 at various times  $T$ , where grid stirring commenced at  $T = 0$  and the neutrally buoyant dye cloud was introduced between  $T = 5$  min and  $T = 5$  min 15 s. (a)  $T = 5$  min 30 s; (b) 6 min 35 s; (c) 12 min 3 s - dye streak introduced; (d) 14 min 45 s - with the distortion of the dye streak revealing the vertically oscillating displacement profile associated with the intrusions.

the grid, and the profiles tend toward a relatively smooth linear gradient. As can be seen in figure 3, this density distribution is also laterally coherent.

The intrusions were not always as regular as depicted in figure 1. As the frequency and/or the amplitude of the grid oscillation was increased for a given density stratification, the motion in the turbulent region became more chaotic (the same effect was evident when the strength of the density stratification was reduced for fixed grid parameters). Eventually, the motion became so energetic that the vertical density oscillations in figures 2 and 3 lost their lateral coherence and evolved rapidly. When this occurred, strong three-dimensional motion was observed in the vicinity of the grid.

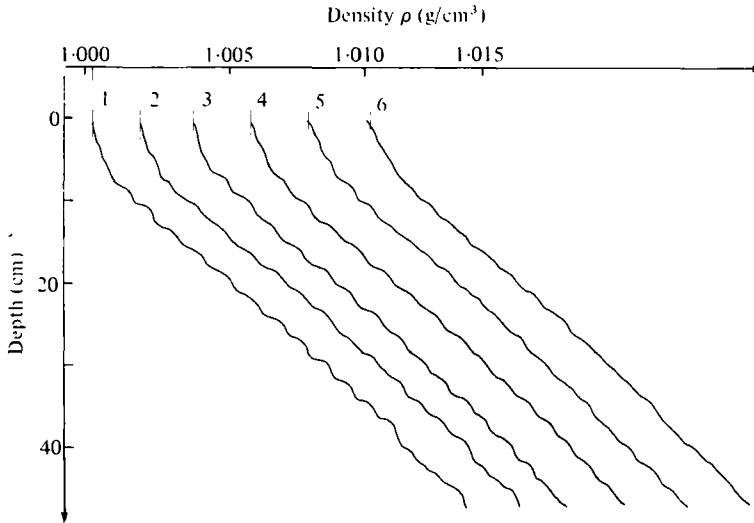


FIGURE 2. Longitudinal density profiles taken in rapid succession along the tank centre line for experiment 21. The first profile (no. 1) was taken approximately 5 min after the commencement of stirring. This profile is undisplaced and the remaining profiles are 'zeroed' by lining up the short vertical bars.

Profile	1	2	3	4	5	6
Distance from grid (cm)	7.5	12.7	17.8	25.4	43.2	61.0

Furthermore, the intrusions tended to meander back and forth across the tank width as they moved out from the grid. The three-dimensional motion was apparently driven by the fluctuating density gradients associated with the irregular step formation.

The multiple intrusion flow pattern, although not always as regular as depicted in figure 1, was a prominent feature of the interior flow of all of the experiments conducted in this study.

A chronological sequence of profiles of conductivity (and hence density) versus depth at one location has the form shown in figure 4. It is clear that the mean density distribution is altered at all heights. At any instant, the distribution depicted in figure 4 is basically the same along the whole tank. The only difference lies in the increasingly pronounced wiggles superimposed over this time-varying mean structure as the oscillating grid is approached. Figure 4 also indicates that the density profiles are asymmetric about the half-depth. The bottom boundary is stationary and the top is a free surface. The local effect of the vertical grid oscillation near these boundaries is complicated, but on the bottom it includes strong corner vortices which must hasten mixing in that region.

By filling the tank slowly it was possible to obtain a two-layer density stratification with an interfacial region of thickness as small as 2–3 cm. Oscillating the grid created a region of intermediate density. This mixed region, in turn, drove a single horizontal intrusion – with a thickness of the same order as that of the interfacial region – out from the grid (see figures 5*a*, *b*). This intrusion rapidly reached the end-wall, and then quickly broke up into a number of weaker intrusions as the interfacial region grew in thickness at the expense of the upper and lower layers (see figure 6).

In situations where the initial stratification was not as sharp as for the case in

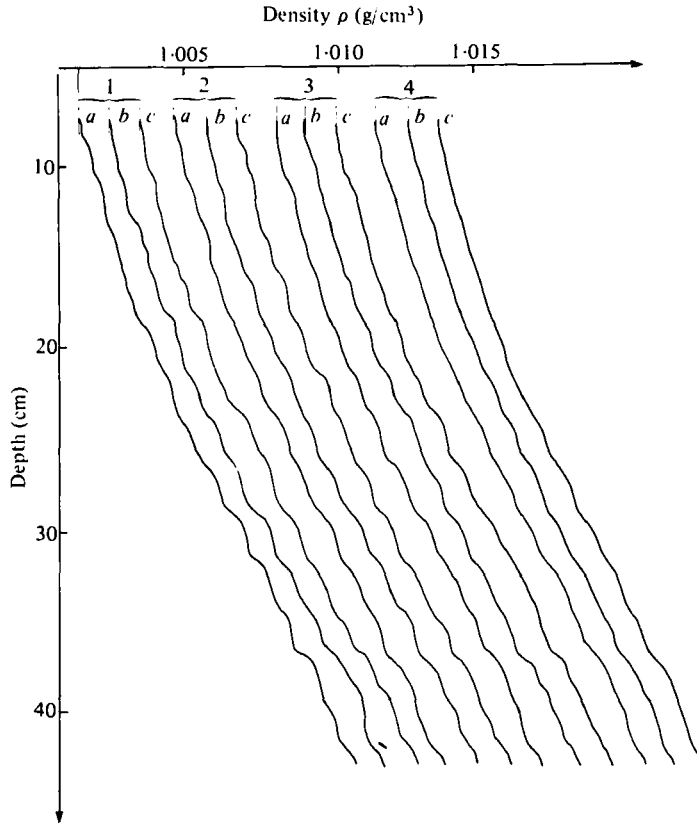


FIGURE 3. Longitudinal and transverse density profiles from experiment 23 – the displaced profiles are ‘zeroed’ by lining up the short vertical bars. First profile taken about 5 min after the commencement of stirring.

Profile	1	2	3	4
Distance from grid (cm)	7.5	15.2	30.5	45.7
Profile	a	b	c	
Distance across tank (cm)	22.9	15.2	7.6	

figure 5(a), the single initial intrusion was not clearly observed. In all cases that started with a single step, multiple intrusions appeared above and below the initial interface; the more remote the intrusion from the interface, the later it appeared. The smoothed density profile evolved as shown in figure 6, in such a way that its central part was approximately linear and had a gradient that decreased more rapidly with time than that which evolved from an initially uniform stratification.

The photographs in figure 1 demonstrate that vigorous turbulent mixing occurs only in a region adjacent to the grid. While no attempt was made to measure any turbulent velocity or density fluctuations, we can note some general features of the turbulent region from shadowgraph observations and conductivity measurements.

With the commencement of stirring, a frontal structure rapidly developed which separated a grid-bound turbulent region from a quiescent interior. The shadowgraph observations indicate that the intrusions moving across this front were very weakly turbulent, but this ‘fossil’ turbulence decayed very rapidly, and the flow was

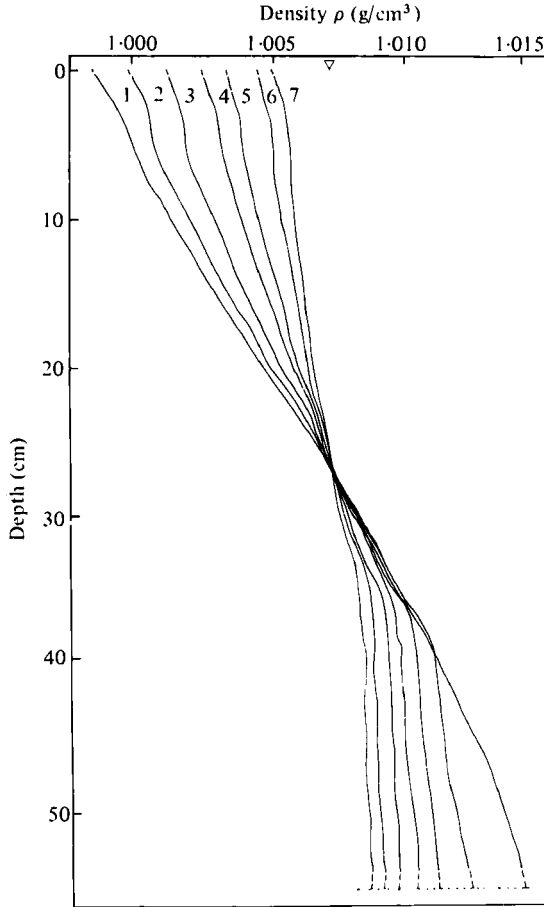
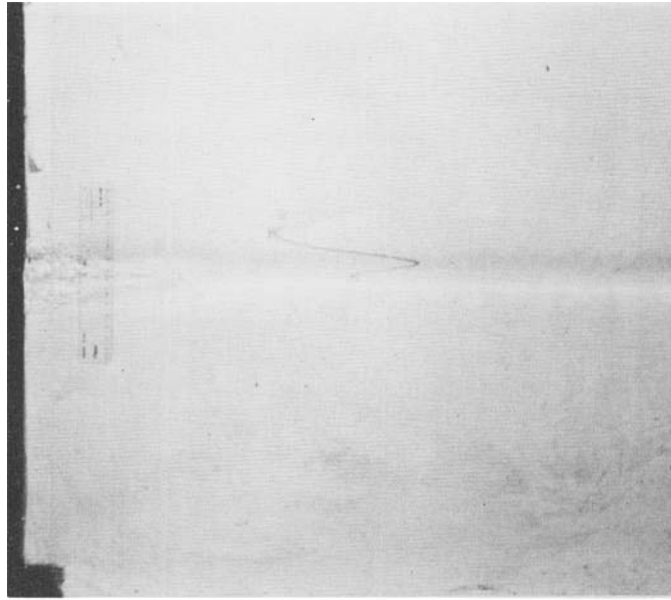


FIGURE 4. Experiment 2 – successive density profiles at  $x = 61$  cm.

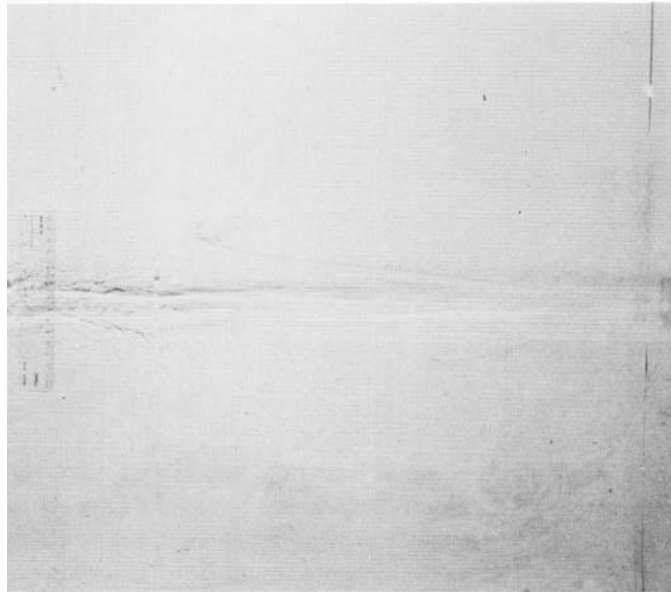
Profile	1	2	3	4	5	6	7
Time (min)	0	23.0	51.5	83.0	110.0	148.0	181.0

essentially laminar in the interior. From the shadowgraph observations, the width of the front  $\delta_T \approx \frac{1}{3}\omega a/N$  for  $\omega a/N$  in the range of 30–120 cm. Since the length of the turbulent region varies with the spanwise location, this estimate is necessarily crude; also, the frontal region defined by the shadowgraph may not coincide with the edge of a turbulent region defined in another way.

A major characteristic of the turbulent region is the creation of steps in the density-versus-depth profiles. Since we did not vary the geometry of the grid, the effects of varying roughness or geometrical proportions of the grooves or bars were not obtained. However, the variation of step height  $h$  (conveniently defined in terms of the intersection of the local tangents to the density-versus-depth curve) with grid frequency of oscillation, amplitude of oscillation and the strength of the density gradient is shown in figure 7. While experiments were conducted beyond the upper range of the scale of the abscissa in figure 7, the turbulent motion became so chaotic that in practice it was not possible to estimate a single characteristic  $h$ . Irregular perturbations about the mean gradient were definitely present, however, for this extended parameter range.



(a)



(b)

FIGURE 5. Shadowgraph photos 10 s (a) and 30 s (b) after the initiation of grid motion ( $\omega = 31.9$  rad/s,  $a = 0.77$  cm,  $N = 2.15$  rad/s). Interfacial region was approximately 4.5 cm thick before stirring commenced.

Although the step size may depend on the bar size  $d$  of the grid (1.27 cms), figure 7 demonstrates that it is not simply fixed by  $d$ . While the data are scattered and of limited range, we note that an average of all data points suggests that

$$\omega a / Nh \simeq 16, \quad (1)$$

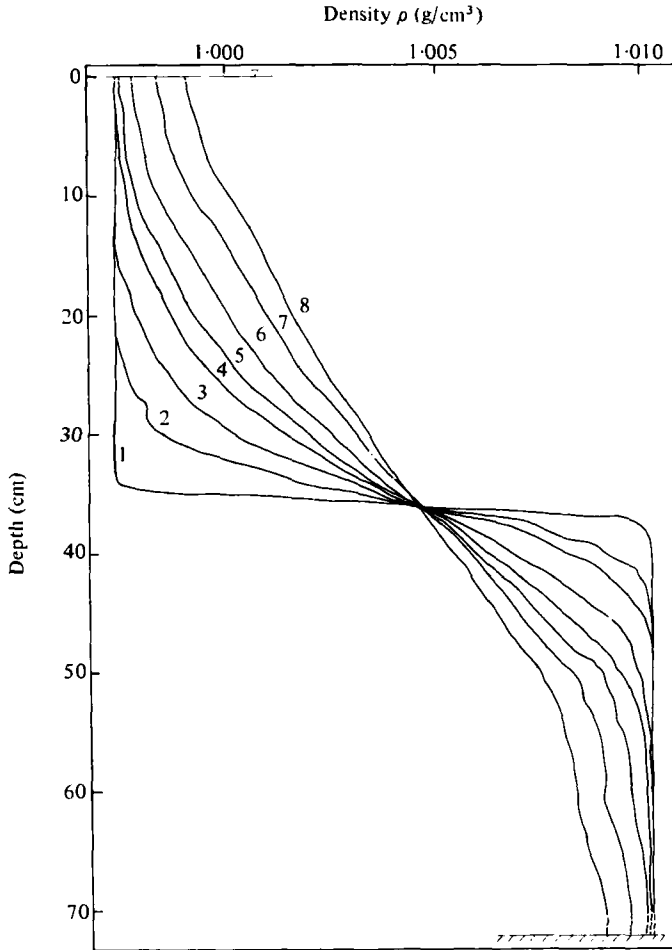


FIGURE 6. Experiment 17 - successive density profiles at  $x = 61$  cm.

Profile	1	2	3	4	5	6	7	8
Time (min)	0	3.6	7.8	15.0	21.5	29.8	43.3	59.2

which has the form of a Froude number based on step height, with the velocity taken as the forcing velocity or grid velocity ( $u_g = \omega a$ ). Since one expects fluid velocities in the turbulent region to be less than this forcing velocity, the tentative suggestion is that a Froude number based on a fluid velocity might be of order unity. In other words, the vertical excursion of a parcel of turbulent fluid is limited to a height  $h$  such that the potential energy gain is a fixed fraction of the initial kinetic energy of the parcel of fluid.

These results are not directly comparable with the earlier laboratory experiments of Thorpe, Hutt & Soulsby (1969) and Chen, Briggs & Wirtz (1971). While the authors did observe multiple intrusions from the boundary into the interior, these intrusions owed their existence to the fact that the density of the working fluid was determined by two components of differing molecular diffusivities in their experiments: temperature and salt.

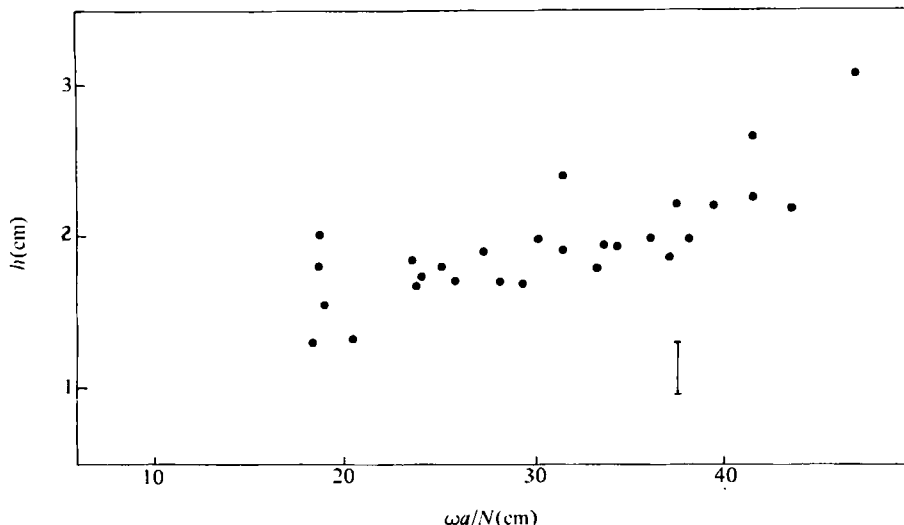


FIGURE 7. Step height versus  $\omega a/N$  (the vertical bar indicates the spatial resolution of the probe).  $N$  was computed from the slope of the background density-versus-depth profiles at mid-depth in the water column.

#### 4. Modelling of the intrusions

In previous work, a number of authors have provided models of a single intrusion of a homogeneous layer into a stratified fluid at rest. The dynamics of the intrusion were governed by either a buoyancy and inertia force balance (e.g. Manins 1976) or a buoyancy and viscosity force balance (e.g. Maxworthy 1972). Imberger, Thompson & Fandry (1976) provide a theoretical description of both these regimes, as well as of a third regime that depends upon diffusion of the stratifying species. But in each of these cases, unlike ours, the intrusions are dependent upon both a fixed source of fluid with an externally controlled volume flux and the interaction of waves with distant boundaries.

The observations discussed in §3 indicate that the intrusive flow in the interior is sometimes three-dimensional. We shall idealize the intrusions as either two-dimensional or axially symmetric around a vertical axis. Although we thereby inevitably lose some numerical accuracy, it is reasonable to expect the dynamics of the intrusions to be sufficiently revealed by these two examples. We shall consider first that the motion is two-dimensional in the  $x$ - and  $z$ -co-ordinates, where the origin of the  $x$ -coordinate is taken as the boundary of the turbulent region, and  $z$  is positive upwards.

As we have seen, the vertical density distribution changes in time. So also must the step size and the intrusions. But these variations occur slowly, so that we shall postpone until later (see §7) a discussion of this gradual approach to uniform density in the tank, and begin here by considering a quasi-steady model of the intrusions in the interior. This assumption is permissible if, as is the case, such a steady state is established in a time small compared with that which characterizes the evolution of the mean-density profile.

Assuming a steady flow, let us decompose the density as

$$\rho_a(x, z) = \rho_0 + \rho_e(z) + \rho(x, z), \quad (2)$$

where  $\rho_a$  is the ambient density,  $\rho_0$  is the reference density,  $\rho_e(z)$  is the equilibrium density about the reference density in the absence of motion, and  $\rho(x, z)$  is the density variation induced by motion. Let us consider a linear density gradient to be present in the absence of motion, i.e.

$$\rho_e(z) = -\beta z, \quad (3)$$

where  $\beta$  is a positive constant, and the Brunt-Väisälä frequency is defined by

$$N = \left( -\frac{1}{\rho_0} \frac{\partial \rho_e}{\partial z} g \right)^{\frac{1}{2}} = \left( \frac{1}{\rho_0} \beta g \right)^{\frac{1}{2}}, \quad (4)$$

where  $g$  is the gravitational acceleration. We shall assume that

$$\rho_e + \rho \ll \rho_0. \quad (5)$$

We make the following simplifying assumptions: firstly, that the flow in the interior is laminar; secondly, that horizontal diffusion is negligible compared to vertical diffusion; and, thirdly, that we may neglect the inertia terms in the momentum equations. However, since the Schmidt number  $= \nu/\kappa$  is of order  $10^3$  for salt-stratified solutions, there is a range of values of  $u$  for which we must retain the nonlinear terms in the species conservation equation.

With these assumptions, the Boussinesq approximation to the governing equations for conservation of mass, species and momentum respectively may be written as

$$\frac{\partial u}{\partial x} + \frac{\partial w}{\partial z} = 0, \quad (6)$$

$$u \frac{\partial \rho}{\partial x} + w \frac{\partial \rho}{\partial z} + w \frac{\partial \rho_e}{\partial z} = \kappa \frac{\partial^2 \rho}{\partial z^2}, \quad (7)$$

$$0 = -\frac{1}{\rho_0} \frac{\partial p}{\partial x} + \nu \frac{\partial^2 u}{\partial z^2}, \quad (8)$$

$$0 = -\frac{1}{\rho_0} \frac{\partial p}{\partial z} - \frac{\rho}{\rho_0} g. \quad (9)$$

We look for a solution to these equations subject to the boundary conditions

$$\rho(0, z) = \Delta \rho \sin kz, \quad (10)$$

$$\rho(x, z) \rightarrow 0 \quad \text{as } x \rightarrow \infty. \quad (11)$$

Under these conditions, the set of nonlinear governing equations (6)–(9) possesses a simple exact solution. This solution, for which the Jacobian  $J$  in (7) is zero (i.e.  $\partial(\rho, \psi)/\partial(x, z) = 0$ , where the stream function  $\psi$  is defined by  $u = \partial\psi/\partial z$  and  $w = -\partial\psi/\partial x$ , is

$$\rho(x, z) = \Delta \rho e^{-\gamma x} \sin kz, \quad (12a)$$

$$u(x, z) = U_0 e^{-\gamma x} \cos kz, \quad (12b)$$

$$w(x, z) = \frac{(\nu\kappa)^{\frac{1}{2}} k^2}{N} U_0 e^{-\gamma x} \sin kz, \quad (12c)$$

$$p(x, z) = \frac{\Delta \rho g}{k} e^{-\gamma x} \cos kz, \quad (12d)$$

where

$$\gamma = \frac{(\nu\kappa)^{\frac{1}{2}} k^3}{N}, \quad U_0 = \frac{\Delta \rho g}{\rho_0 N} \left( \frac{\kappa}{\nu} \right)^{\frac{1}{2}}. \quad (13)$$

The solution (12) indicates that the amplitude of the density perturbations imposed at the boundary decays exponentially with distance  $x$ . A measure of this decay rate is given by the  $e$ -folding length

$$L_e = \frac{1}{\gamma} = \frac{N}{(\nu\kappa)^{\frac{1}{2}} k^3}. \quad (14)$$

We may compare the prediction in (14) with the laboratory experiments. For example, from the data (see figure 2)  $N = 0.58$  rad/s,  $\nu = 10^{-6}$  m<sup>2</sup>/s,  $\kappa = 1.3 \times 10^{-9}$  m<sup>2</sup>/s and  $k = 2.62 \times 10^3$  m<sup>-1</sup>; then (14) yields  $L_e = 90$  cm. The instrument resolution becomes important when detecting very small perturbations about the mean-density gradient, so that the experimental evaluation is not very accurate. The profiles in figure 2 indicate  $L_e \sim 60$  cm. With a note of caution about the possible three-dimensional nature of the flow, we can conclude that the theory of the intrusive flow, summarized by (12), is a plausible description of the laboratory experiments.

If the geometry were such that the turbulence was generated near a quasi-cylindrical mixing region, a solution in terms of cylindrical polar co-ordinates would be more appropriate. If we assume the flow to be axisymmetric, then the governing equations in cylindrical polar co-ordinates are

$$\frac{1}{r} \frac{\partial}{\partial r} (ru) + \frac{\partial}{\partial z} (w) = 0, \quad (15a)$$

$$w \frac{\partial \rho_e}{\partial z} = \kappa \frac{\partial^2 \rho}{\partial z^2}, \quad (15b)$$

$$0 = -\frac{1}{\rho_0} \frac{\partial p}{\partial r} + \nu \frac{\partial^2 u}{\partial z^2}, \quad (15c)$$

$$0 = -\frac{1}{\rho_0} \frac{\partial p}{\partial z} - \frac{\rho}{\rho_0} g. \quad (15d)$$

Proceeding as before, and looking for a solution in which  $\rho(r, z) \rightarrow 0$  as  $r \rightarrow \infty$ , the solution is given by

$$\rho(r, z) = BK_0(\gamma r) \sin kz, \quad (16a)$$

$$u(r, z) = U_0 K_1(\gamma r) \cos kz, \quad (16b)$$

$$w(r, z) = \frac{U_0 \gamma}{k} K_0(\gamma r) \sin kz, \quad (16c)$$

$$p(r, z) = \frac{Bg}{k} K_0(\gamma r) \cos kz, \quad (16d)$$

where  $K_0$  and  $K_1$  are modified Bessel functions of order 0 and 1 respectively.  $\gamma = (\nu\kappa)^{\frac{1}{2}} k^3 / N$ ,  $U_0 = (Bg/\rho_0 N) (\kappa/\nu)^{\frac{1}{2}}$ , and  $B$  is a constant given by  $B = \Delta\rho/K_0(\gamma r_T)$ . The radius  $r_T$  is the radius of the shore-bound mixing region.

#### 4.1. Vertical mass flux and vertical mixing

Consider the interior of the fluid in our laboratory experiment. The vertical mass flux  $F$  per unit area is given by

$$F = w\rho_e + w\rho - \kappa \frac{\partial \rho_e}{\partial z} - \kappa \frac{\partial \rho}{\partial z}. \quad (17)$$

Substituting (12) into (17), and defining an average vertical mass flux  $\bar{F}$  by

$$\bar{F} = \frac{k}{2\pi} \int_0^{2\pi/k} F(z) dz,$$

we find that

$$\bar{F} = (\Delta\rho k\kappa) e^{-\gamma x} + \frac{1}{2} \left( \frac{\Delta\rho k}{N} \right)^2 \frac{\kappa g}{\rho_0} e^{-2\gamma x} - \kappa \frac{\partial\rho_e}{\partial z}. \quad (18)$$

We may put an upper bound on the mass flux  $F$ . The density perturbation  $\Delta\rho$  is dependent on the strength of the background density gradient  $\partial\rho_e/\partial z$ , and if we rule out gravitational instability the maximum value  $\Delta\rho$  can attain for a given vertical wavelength  $2\pi/k$  is

$$\Delta\rho = -\frac{1}{2} \frac{\partial\rho_e}{\partial z} \frac{2\pi}{k}. \quad (19)$$

Substituting (19) into (18) yields

$$\bar{F} = -\pi\kappa \frac{\partial\rho_e}{\partial z} e^{-\gamma x} - \frac{1}{2}\pi^2 \frac{\partial\rho_e}{\partial z} \kappa e^{-2\gamma x} - \kappa \frac{\partial\rho_e}{\partial z}. \quad (20)$$

It is evident that this positive (i.e. upward) mass flux decays rapidly with  $x$ . The maximum value occurs as  $x \rightarrow 0$ , and if we define an eddy diffusivity  $\epsilon$  by

$$\bar{F} = -\epsilon \frac{\partial\rho_e}{\partial z}, \quad (21)$$

then substituting (21) into (20) yields

$$\epsilon_{\max} = (\pi + \frac{1}{2}\pi^2 + 1)\kappa = 9.08\kappa.$$

In other words, the total vertical eddy diffusivity, due to an intrusive process in which inertia plays no role and which remains gravitationally stable everywhere, has a maximum value of only 9.08 times the molecular diffusivity of the stratifying species. The observed eddy diffusivities in the experiment (§5) are of order  $10^3$  times molecular values. We conclude that, although the multiple intrusions are a prominent feature of the experiments, they make a negligible direct contribution to the observed net vertical mass transport.

We are led to surmise that the approach to homogeneous conditions, which is essentially independent of horizontal location, must therefore be, at least in the interior, the result of slow *vertical* advection. This is the subject of §6.

## 5. Measurement of vertical mass transport

Consider now a new co-ordinate system with the origin at the grid;  $x$  is now distance from the grid, and  $z$  is distance measured upwards. Our fluid domain therefore includes the turbulent grid-bound mixing region. We shall represent this turbulent flow by the usual Reynolds decomposition. Since we are concerned with mixing processes in which the mean density gradient itself changes, we shall now decompose the density as  $\rho_a = \rho_0 + \rho + \rho'$ . Then integrating the conservation-of-species equation from  $x = 0$  to  $x = L$  (the tank length), and integrating from some elevation  $z_0$  to  $z = H$  (the free surface) yields

$$F = \left[ \frac{d}{dt} \int_{z_0}^H \rho dz \right] L, \quad (22)$$

where  $F$  denotes the net mass flux across the horizontal plane  $z = z_0$ , and we have used the observation that  $\rho$  is only a weak function of  $x$ . If we neglect molecular diffusion across the plane  $z_0$  then

$$F = \left[ \int_0^L \overline{w' \rho'} dx \right] \Big|_{z_0},$$

where the overbar denotes a time average. Equation (22) states that the mass transport across the boundary  $z = z_0$  leads to an increase in mass in the fluid volume with lower boundary  $z_0$ . We could define an eddy diffusivity by

$$F = -\epsilon \frac{\partial \rho}{\partial z} \Big|_{z_0}. \quad (23)$$

But the data indicate that  $F$  is not proportional to  $\partial \rho / \partial z$  (see (25)). The definition in (23) implies a local turbulent diffusion across any horizontal plane, an implication which is grossly misleading. We will therefore take  $F$  to be the fundamental dependent variable.

The experimental mass flux  $F$  was evaluated by using a finite-difference approximation to (22), i.e.

$$F = \left[ \int_0^L \overline{w' \rho'} dx \right] \Big|_{z_0} \simeq \frac{\left[ \int_{z_0}^H \rho dz \Big|_{t+\Delta T} - \int_{z_0}^H \rho dz \Big|_t \right] L}{\Delta T}. \quad (24)$$

Thus from any two traces of conductivity (and hence density) versus depth taken at time  $t = \Delta T$  apart, one may readily compute  $F$  from (24). With  $F$  as the fundamental dependent variable, the independent variables investigated in this study were the ambient density stratification at the lower boundary, the frequency of oscillation of the grid, the amplitude of oscillation of the grid, the tank length and the water depth.

The mass flux through the centre plane  $z = \frac{1}{2}H$  depends on the density gradient at the same height. In order to exhibit this dependence, the lower limit of integration in the finite-difference approximation (24) was taken as  $z_0 = \frac{1}{2}H$ . The slope of the tangent to the curve  $\rho = \rho(z)$  at  $z_0 = \frac{1}{2}H$  was evaluated from the original traces at time  $t$  and  $t + \Delta T$ . The average of these two slopes was then taken as the characteristic density gradient, corresponding to the average mass flux over  $\Delta T$  computed from (24). The data from five experiments are summarized in figure 8.

The data plotted in figure 8 come from experimental runs with both linear and two-layer initial stratifications. Data points for the second case, for times in which the density gradient vanishes before the upper and lower boundaries are reached, have been marked differently. Within experimental scatter, the dependence of  $F$  on  $N$  appears to be the same for both sets of points. This suggests rather strikingly that  $F$  at  $z = \frac{1}{2}H$  depends only upon  $N$  at the same height. In other words, the transport of salt across  $z = \frac{1}{2}H$ , which as argued in §4 must take place almost entirely in the turbulent region, is locally controlled by the density gradient.

We may easily compute a vertical eddy diffusivity, as defined in (23), from these data. From figure 8, for example, if  $N^2 = 0.5 \text{ rad}^2/\text{s}^2$ ,  $F = 3 \times 10^{-4} \text{ kg/s m}$ , and noting that  $L = 1.83 \text{ m}$ , the eddy diffusivity has a value of  $\epsilon = 3.2 \times 10^{-6} \text{ m}^2/\text{s}$ . However, as we noted in §4, and as we shall discuss further in §6, this apparent diffusivity of the fluid is a result of diffusion within the turbulent zone only and has limited significance.

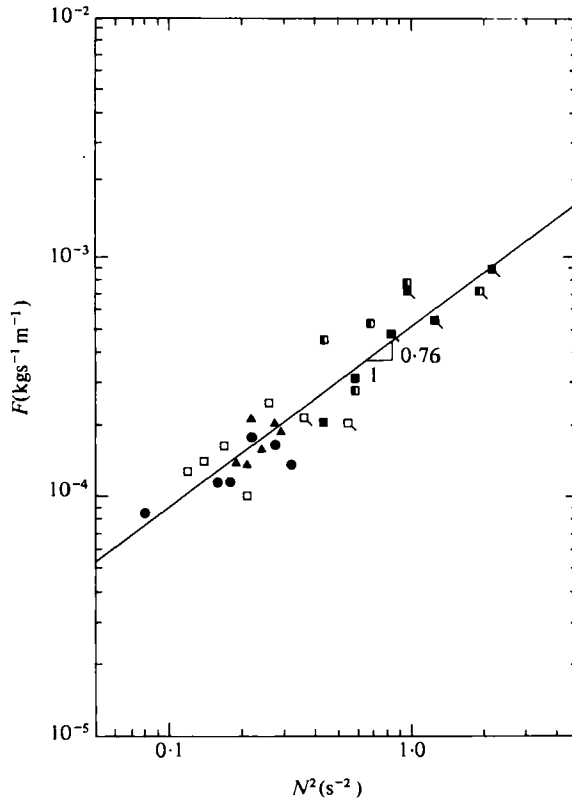


FIGURE 8. Vertical mass flux as a function of  $N^2$ . Data points from the two-layer experiments for times in which the density gradient vanishes before the upper and lower boundaries have been reached are denoted by an additional 'tail' (e.g.  $\blacksquare$ ).  $\blacktriangle$ , experiment 1;  $\bullet$ , 2;  $\square$ , 3;  $\blacksquare$ , 4;  $\blacksquare$ , 5.

In order to compare experiments with different grid oscillation frequencies, for example, it is convenient to introduce an auxiliary variable  $F^*$  defined by

$$F^* = \frac{1}{N_2^2 - N_1^2} \int_{N_1^2}^{N_2^2} F(N^2) d(N^2).$$

Then, using the data from one experiment, we have a finite number of data points on the curve of  $F$  vs.  $N^2$ . Any number of experiments may then be compared by computing  $F^*$  over the range of integration common to all experiments. The dependence of  $F^*$  on frequency  $\omega$  and amplitude of oscillation  $a$  is shown in figures 9 and 10 respectively.

The results from three experiments in which the length of the tank was varied are shown in table 2. The data indicate that, to the accuracy of measurement of mass flux, there is no dependence of  $F^*$  on  $L$ . The implication of this result is discussed in § 6. The design of the experiment did not allow for the total depth of the fluid to be varied sufficiently to infer the effect of depth on mass flux.

These results lead to a best fit to the data given by

$$F \propto \omega^{1.6} a^{2.7} \left( \frac{\partial \rho}{\partial z} \right)^{0.76}. \quad (25)$$

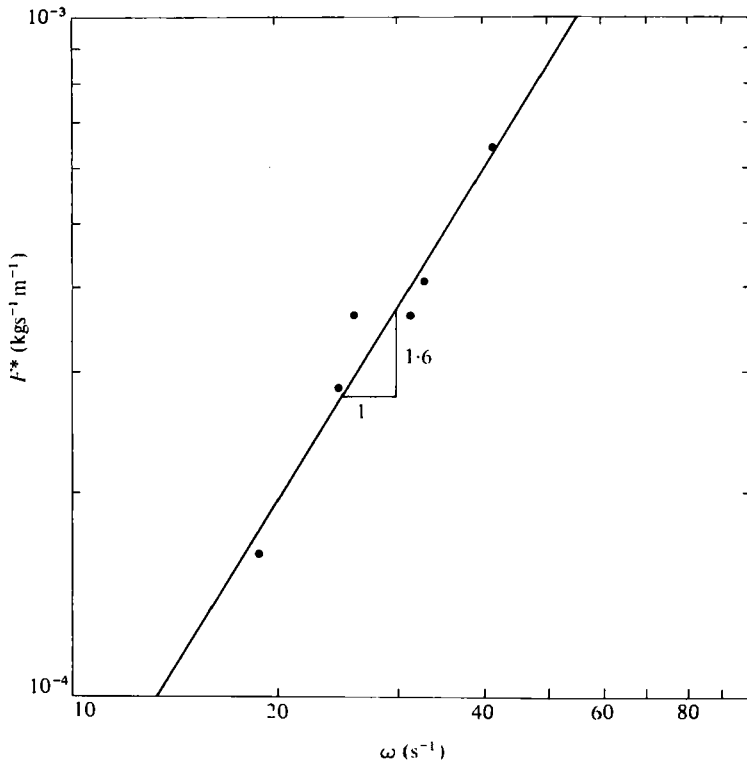


FIGURE 9. Vertical mass flux versus frequency of grid oscillation.  $N^2$  from  $0.4$ – $2.3 \text{ s}^{-2}$ .

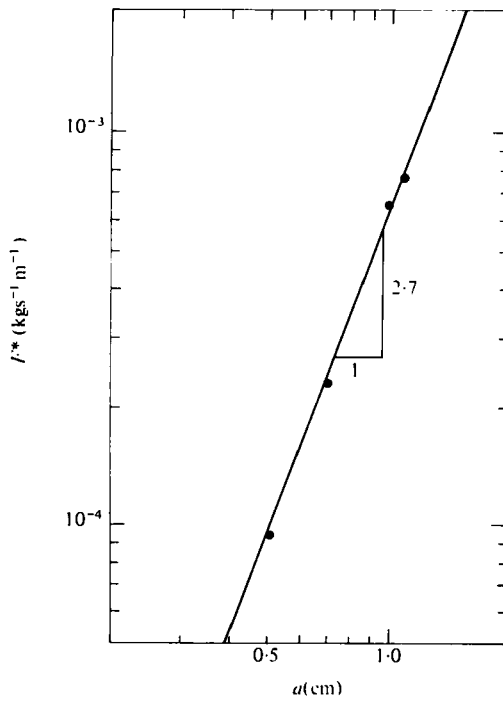


FIGURE 10. Vertical mass flux versus amplitude of oscillation.  $N^2$  from  $0.45$ – $2.0 \text{ s}^{-2}$ .

Experiment	$F^*$ ( $\times 10^4$ ) kg/s m	$L$ (m)	$H$ (m)	$N^2$ ( $s^{-2}$ )
16	6.6	0.92	0.70	
17	7.2	1.25	0.71	0.5 $\rightarrow$ 2.0
8	7.0	1.83	0.70	

TABLE 2. Mass flux as a function of container size

In order to summarize all of these results from the experiments, let us make two hypotheses. Our first hypothesis is that the true form of (25) is

$$F \propto \omega^{1.5} a^{3.0} \left( \frac{\partial \rho}{\partial z} \right)^{0.75}. \quad (26)$$

In order to make the step from (25) to (26), we must accept the fact that the experimentally determined exponents in (25) can be in error by at most 10%. Considering the restrictions on the range of the data and the number of data points used in deriving these correlations, such an error is quite plausible. Our second hypothesis is that

$$F = F \left( \omega, a, \frac{\partial \rho}{\partial z}, \rho_0, g \right).$$

The notable omissions from this list of independent variables are the grid roughness  $d$ , the aspect ratio  $H/L$ , and possibly the molecular diffusivity  $\kappa$  of the stratifying species. Other grid-stirring experiments (e.g. Hopfinger & Toly 1976), although done for vastly different experimental configurations, have shown a dependence of grid-generated turbulence on the grid roughness or mesh size. Furthermore, in a turbulent mixing process, the diffusivity of the stratifying species can have an effect on the overall mixing rate in some situations (see Turner 1973, p. 295). But if we accept these two hypotheses, simple dimensional reasoning indicates that the mass flux is given by

$$F \sim \omega^{1.5} a^{3.0} \left( \frac{\partial \rho}{\partial z} \right)^{0.75} \left( \frac{\rho_0}{g} \right)^{0.25},$$

or

$$F \sim \left( \frac{\rho_0}{g} \right) \omega^{1.5} a^{3.0} (N^2)^{0.75}. \quad (27)$$

If we assume that (27) is valid, the data from all the experiments in this study can be plotted as in figure 11. Although we must view these simple dimensional arguments as incomplete, especially in the absence of a secure understanding of the mixing mode, we see from figure 11 that they do agree with the experimental observations over the considerable range of parameters involved.

## 6. The mixing mode

We come now to the central question raised by the experiment: how is the initial density gradient eventually destroyed? This question has two interrelated aspects: firstly, the diffusive properties of the turbulence near the grid, and, secondly, the mechanism by which at any height the non-turbulent fluid undergoes a change in density almost simultaneously with the turbulent fluid.

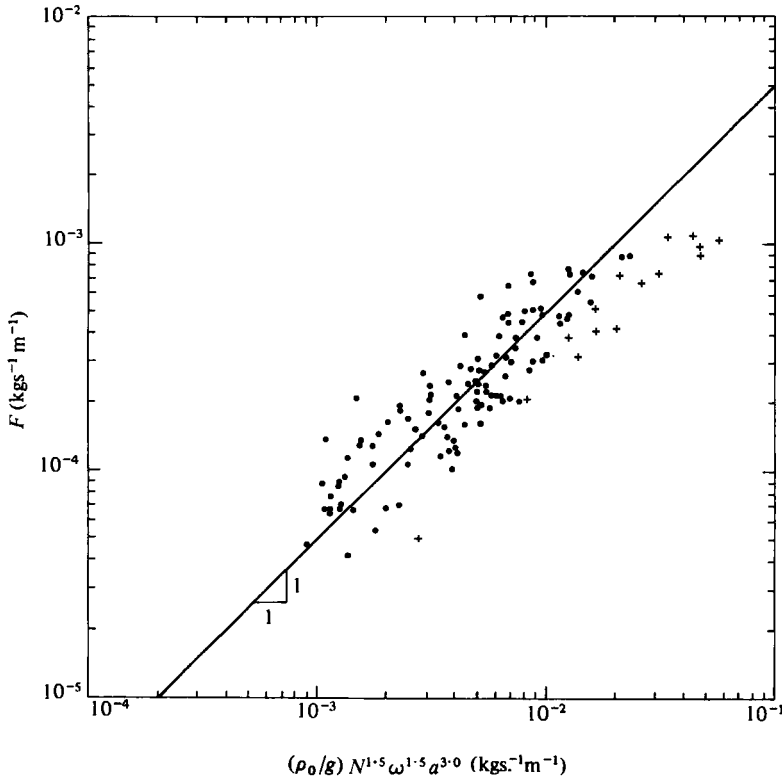


FIGURE 11. Summary of all experiments. The crosses denote points considered uncertain due to difficulties in estimating a characteristic slope of the density gradient. The line of slope 1 was drawn by eye for comparison.

In addition to the localized mixing responsible for the steps, the effect of the turbulence created by the vertically oscillating grid must be to induce a systematic transport of salt vertically upwards through the steps for as long as a vertical density gradient exists. It is the vertical divergence of this transport that causes local changes in the density. Thus, if the effective vertical diffusion coefficient and the density gradient were independent of height, no change in density would take place in the turbulent region and, in turn, no motion would be induced in the statically stable interior.

On the other hand, if (i) the vertical density gradient is not uniform (as in the two-layer experiment), (ii) horizontal boundaries prevent or alter vertical fluxes, or (iii) the vertical diffusion coefficient varies with height, then the resulting divergence of the vertical flux will alter the local density, and hence the density gradient in the turbulent region. We infer from the experimental observations of the slow variation of the density profile towards a situation of uniform density that one or more of these attributes of the turbulent flow is always present. If the density of the interior fluid were to remain constant, horizontal differences in density would occur between the interior and the turbulent region adjacent to the grid.

Let us now consider the second aspect of our question above: the mechanism of adjustment of density of the non-turbulent interior fluid. Suppose that at one vertical

boundary of a linearly stratified fluid the density gradient is suddenly decreased by a small amount, and the boundary condition maintained thereafter. How does the fluid adjust to its new boundary condition, and what is the time  $T_1$  required for this adjustment? If, on the other hand, the boundary conditions were changed continuously at a rate characterized by a time  $T_2$ , and if  $T_1 \ll T_2$ , then we would conclude that there would be no noticeable difference between the density at the boundary and that in the interior at the same height for any time.

The model problem above has been discussed by Veronis (1970). He pointed out that it is analogous to the (negative) spin-up problem originally studied in its linear form by Greenspan & Howard (1963). It is applicable in the present context, albeit with a few differences. Firstly, the vertical density gradient is not, in general, independent of  $z$ , as in the model problem. Secondly, the stratifying agent has a horizontal flux through the vertical boundary in the model problem, whereas in our experiment it has a vertical flux along the boundary for which the turbulence is responsible. Thirdly, the diffusivity of salt, important in the near balance between horizontal diffusion and vertical advection of density in the buoyancy layer (see below), is due to turbulent small-scale motion – i.e. it is an eddy diffusivity about which we know very little. These complications conspire to put a detailed analytic solution out of our reach. We can, however, make estimates of the time scales involved and thereby gain some understanding of the adjustment mechanism.

The basic element of the model problem discussed by Veronis (1970) is that a quasi-steady balance is rapidly established (in a time of order  $N^{-1}$ ) between the vertical advection of the density gradient and the horizontal diffusion of the local density anomaly in the buoyancy layer adjacent to the grid. Since, according to the boundary conditions, the density anomaly  $\delta\rho$  is then an increasing function of height, the vertical component of velocity is vertically divergent, which leads to a general horizontal outflow into the interior. Since this horizontal motion vanishes at the other (passive) vertical boundary,  $\partial w/\partial z > 0$  by continuity, and a vertical current, positive above and negative below the mid-plane, slowly increases the scale height of the density gradient in the interior according to

$$\frac{\partial}{\partial t} \left( \frac{\partial \rho}{\partial z} \right) = - \frac{\partial}{\partial z} \left( w \frac{\partial \rho}{\partial z} \right) \simeq - \frac{\partial w}{\partial z} \frac{\partial \rho}{\partial z}.$$

The flow pattern is sketched in figure 12.

Following Veronis (1970), the ‘mix-up’ time  $T_1$  of the interior fluid in response to a small decrease in density gradient at the boundary may be written as

$$T_1 \sim \frac{L}{N^{\frac{1}{2}} \epsilon_H^{\frac{1}{2}}},$$

where  $N$  is the initial Brunt–Väisälä frequency and  $\epsilon_H$  is the effective horizontal turbulent diffusivity. We have assumed here that the turbulent Schmidt number, equal to the ratio of the eddy viscosity to the turbulent diffusivity, both in the horizontal direction, is of order unity in the turbulent zone.

We may evaluate  $\epsilon_H$  crudely from the vertical flux of salt at  $z = \frac{1}{2}H$ . At that height (see figure 12), the vertical velocity vanishes in both the interior and the turbulent layer. Thus all the vertical transport occurs by vertical turbulent diffusion within the turbulent layer. The vertical diffusivity there is then, on the average, the one computed

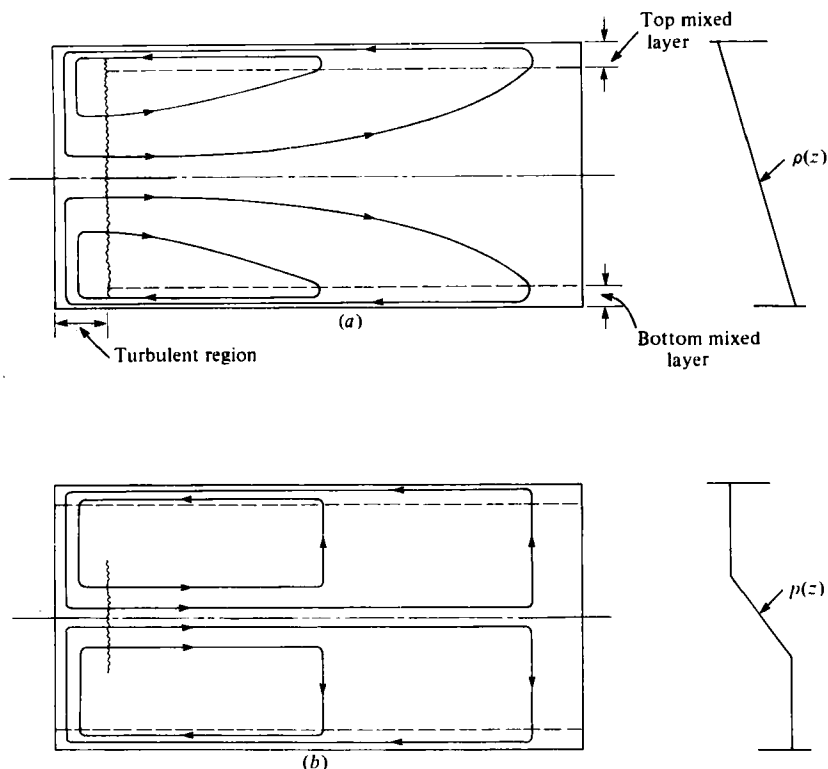


FIGURE 12. Schematics of the circulation in experiments with (a) an initial linear density stratification, and (b) an initial discontinuous stratification.

for the whole tank in § 5 multiplied by the ratio  $R = L/\delta_T$ , where  $\delta_T$  is the width of the turbulent zone. We shall take  $R \sim 10$ , and, noting that the horizontal diffusivity is not likely to be smaller than the vertical one, we finally obtain  $\epsilon_H \sim 3 \times 10^{-5} \text{ m}^2/\text{s}$ . Then, with typical values  $L = 1.83 \text{ m}$  and  $N = 0.5 \text{ rad/s}$ , we get

$$T_1 \simeq 472 \text{ s} \simeq 8 \text{ min.}$$

As we shall see in § 7, the time  $T_2$  required for the fluid to be mixed homogeneously in the experimental tank is considerably larger than this estimate. Thus the model successfully explains why we found no appreciable horizontal density gradients, and provides a plausible mode of mixing throughout the tank.

In the model, the difference between the vertical density gradients at the boundary and those in the interior is independent of height, and thus the horizontal velocity  $u_0$  of the fluid as it leaves the buoyancy layer is uniform. The velocity field in the interior is then of the form (see figure 12a)

$$u = u_0 \left[ 1 - \frac{x}{L} \right], \quad w = u_0 \left[ \frac{z}{L} \right].$$

For a more general case, the horizontal velocity is a function of height, and in particular vanishes at heights where the density gradient has no tendency to change. Thus for the two-layer case,  $u = 0$  and  $w$  is constant above and below the gradient region (see figure 12b). In general, the differential vertical advection responsible for the

adjustment of the interior fluid density to that in the turbulent region occurs only at the height where it is needed.

We note, however, that the model does not help us in predicting the shape of the evolving density profile. When the density gradient is initially near-uniform, for example, one would expect the density near the grid to depart from its initial value at points where the density profile is curved (e.g. near top and bottom boundaries in a 'perfectly' linear stratification). Figure 4 is ambiguous in this respect: in the top half of the tank the profiles are almost straight, although their gradient is steadily changing. This suggests that the divergence of the vertical flux of salt in the turbulent region is not given by a simple one-dimensional diffusion equation. A complete description of the evolving density profile must also incorporate some details of the undocumented, but experimentally obvious, agitation of the flow in the corner regions. For the moment, the shape of the evolving density profile remains unaccounted for.

## 7. Experimental evaluation of mixing time and vertical mixing coefficient

### 7.1. Mixing time

We note that our data provide information about the time required to mix the tank. From (22) and (27) we can write

$$\left[ \frac{d}{dt} \int_{\frac{1}{2}H}^H \rho dz \right] L = B \left( \frac{\rho_0}{g} \right) \omega^{1.5} a^{3.0} N^{1.5}, \quad (28)$$

where  $N$  is evaluated at  $\frac{1}{2}H$ , and the constant  $B \simeq 0.05$  from figure 11. Let us consider a situation in which the density is given by

$$\rho(z, t) = -\beta(t)z \quad \text{where} \quad N^2 = \frac{g}{\rho_0} \beta.$$

That is, we are considering the case where the density gradient is changing slowly, but for the sake of simplicity the profile is assumed to remain linear. If at some initial time  $t_1$  we denote the slope and Brunt-Väisälä frequency by  $\beta_1$  and  $N_1$  respectively, we may write (28) as

$$\left[ \frac{d}{dt} \int_{\frac{1}{2}H}^H \beta_1(t)z dz \right] L = -B \left( \frac{\rho_0}{g} \right) \omega^{1.5} a^{3.0} N_1^{1.5},$$

i.e. 
$$\frac{d\beta_1}{dt} = - \left( \frac{8B}{3} \right) \left( \frac{\rho_0}{g} \right) \frac{\omega^{1.5} a^{3.0} N_1^{1.5}}{H^2 L},$$

and dividing through by  $\beta_1 = (\rho_0/g)N_1^2$  yields

$$\frac{1}{\beta_1} \frac{d\beta_1}{dt} = -\frac{8}{3} B \frac{\omega^{1.5} a^{3.0}}{N_1^{0.5} H^2 L}. \quad (29)$$

Thus if we define  $T_2$  as the time required to change the density gradient, we see from (29) that

$$T_2 \sim 7.5 \frac{N_1^{0.5} H^2 L}{\omega^{1.5} a^{3.0}}, \quad (30)$$

where we have taken  $B = 0.05$ . For the laboratory experiments, typical values of the parameters are  $N_1 = 0.5$  rad/s,  $H = 0.7$  m,  $L = 1.83$  m,  $\omega = 30$  rad/s and  $a = 10^{-2}$  m, which implies that  $T_2 \sim 3 \times 10^4$  secs. This is substantially larger than  $T_1$ , as remarked in §6.

### 7.2. Vertical mixing coefficient

The results of our experiment suggest that the net vertical mass flux is only indirectly associated with a vertical diffusion mechanism. Nevertheless, the apparent effect of the grid-created motion may be described by an effective vertical diffusivity  $\epsilon$  defined by (23). In view of (28), this takes the form

$$\epsilon = B \frac{\omega^{1.5} a^3}{LN^{0.5}},$$

where the measurements indicate that  $B \simeq 0.05$ . The dependence on  $\omega$  and  $a$  is peculiar to our experiment, and takes the place of turbulence parameters. But the dependence of  $\epsilon$  on density gradient, which should have more general validity, is not predicted by a simple model based on energy arguments (e.g. Garrett (1979*b*), which predicts  $\epsilon \propto N^{-2}$ ). It is, of course, of interest to know how the experimental results could be used to predict vertical mixing rates in nature, but such an extension of the laboratory results is clearly premature for several reasons. One would first need to characterize the grid-generated turbulence and establish more conclusively the details of the mixing process in the laboratory experiments. Furthermore, the range of parameters chosen for the laboratory experiment did not allow us to study flows in which inertia may be important in governing the motion of the intrusions away from the immediate vicinity of the boundaries. For the field data, one would need to speculate on the cause and nature of boundary turbulence (seiche, mean current shear, etc.). Finally, as shown below, neither horizontal advection by large-scale current systems nor Coriolis forces can apparently be neglected in interpreting field observations.

## 8. Field observations of boundary mixing

Over fifteen years ago, Munk (1966) drew attention to the possible importance of boundary mixing in the ocean. More recently, several field experiments in both oceans and lakes have yielded data which has been interpreted as evidence of this phenomenon. The oceanic data have been summarized by Armi (1978). Detailed measurements have been reported by Wunsch (1972), Hogg, Katz & Sanford (1978), Gregg & Sanford (1980) and Armi & D'Asaro (1980) for the Atlantic Ocean and by Caldwell, Brubaker & Neal (1978) for Lake Tahoe. It would seem natural to ask whether our work sheds some light on this data, thus providing a model for its interpretation. It is instructive, then, to assume that the lake and oceanic observations pertain to a simple viscous-buoyancy force balance and to examine the validity of the assumption in the light of the available data.

Figure 13 shows a series of profiles of temperature with depth taken by Caldwell *et al.* (1978) in the north-west part of Lake Tahoe. The profiles clearly exhibit an increased step-like structure in successive profiles as the shore is approached and we note that the largest steps have a height of 3 m. Then, with a vertical wavenumber  $k = \frac{3}{2}\pi \text{ m}^{-1}$ , and using molecular values of the transport coefficients, (13) and (14) predict an  $e$ -folding length  $L_e = 3.8 \text{ km}$  and a velocity  $U_0 = 1.5 \text{ cm/s}$ . This maximum value of the buoyancy-generated horizontal velocity is rather small compared with likely nearshore currents driven by forces independent of the buoyant collapse of the steps. Further, there is the possibility of Coriolis forces being important in

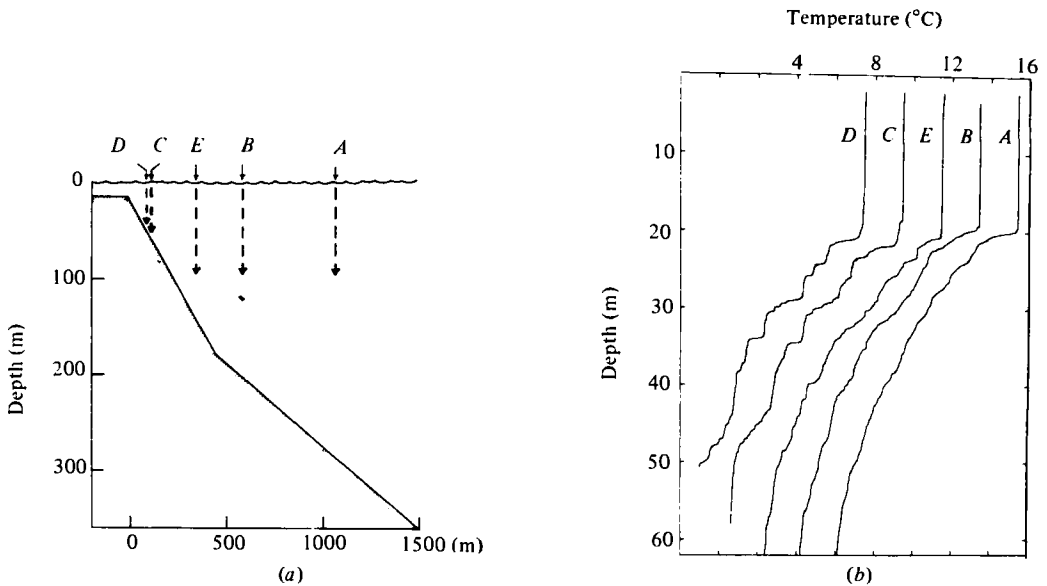


FIGURE 13. (a) Locations of temperature microstructure profiles. Stations are in the northwest part of the lake, on a bearing of  $110^\circ$  magnetic from Lake Forest Coast Guard Station about 3 km from station (from Caldwell *et al.* 1978). (b) Profiles of temperature *vs.* depth. Scale is given for profile A, others being displaced  $2^\circ$  progressively to left. Mixed-layer temperature does not vary appreciably between stations. Order of letters represents order in which stations were taken, all within 2 h in time (from Caldwell *et al.* 1978).

the data. We can generalize our equation (8), and, using (9) to eliminate pressure, write

$$-\frac{g}{\rho_0} \frac{\partial \rho}{\partial x} = f \frac{\partial v}{\partial z} + \nu \frac{\partial^3 u}{\partial z^3}, \quad (31)$$

$$-\frac{g}{\rho_0} \frac{\partial \rho}{\partial y} = -f \frac{\partial u}{\partial z} + \nu \frac{\partial^3 v}{\partial z^3}, \quad (32)$$

where  $v$  is the velocity in the longshore direction (i.e.  $y$ ) and  $f$  is the Coriolis parameter. Estimating  $u$  by  $U_0 = 1.5$  cm/s above, then (31) implies that for Coriolis to be unimportant  $v$  must be no greater than  $2.1 \times 10^{-3}$  cm/s. But this result then implies that the magnitude of the Coriolis term in (32) is much larger than the viscous term, and a balance of forces can only be achieved by large density gradients in the longshore direction (of the order of  $1.7^\circ\text{C}/\text{km}$ ). Persistent gradients of this magnitude seem unlikely, and these order-of-magnitude arguments suggest a simple viscous-buoyancy balance is unlikely to prevail in these observations.

As a second example, let us consider the data taken off the island of Bermuda. Observations made by Wunsch (1972), Hogg *et al.* (1978) and Gregg & Sanford (1980) indicated that the mixing was generated by the interaction of a mean flow with the rough bottom topography on the sloping sides of the island. This mean flow was apparently driven by Gulf Stream rings in the proximity of the island. The data indicate that boundary mixing was not uniformly distributed around the island. Rather, boundary mixing was most pronounced in three distinct patches of finite size attached to the sloping sides of the island. These patches occurred where the induced

flow, due to the Gulf Stream rings, impinged on the shore. The patchiness suggests that any multiple intrusive flow away from the shorebound mixing regions would be three-dimensional.

The axisymmetric version of our model (16), with a step height  $h$  of 15 m (from Gregg & Sanford's figure 3) predicts  $U_0 = 3.6$  cm/s. When compared with typical observed current speeds of order 10 cm/s (Hogg *et al.* 1978), it is clear that these large-scale currents are likely to influence strongly the spatial distribution of boundary-mixed fluid by advecting the mixed fluid away from the boundaries. Using a similar argument to that above, one can conclude that Coriolis forces are also likely to be important.

We conclude that our experiment and the proposed model of the flow cannot be compared with these field observations as the data suggests that Coriolis forces are important and that it is likely that currents exist acting to advect the boundary-mixed water away from the shore-bound mixing regions.

## 9. Conclusions

The laboratory experiment indicated that turbulence is confined to a region adjacent to the oscillating grid. Mixing near the grid creates a step-like structure in an initially smooth profile of density with depth. The steps are characterized by a Froude number based on grid velocity, step height, and ambient stratification of approximately 16. Once created, these steps drive multiple intrusions away from the boundary and into the non-turbulent interior of the fluid. A compensating return flow carries fluid from the interior into the turbulent mixing region.

Dye observations suggest that little vertical mass transport occurs in the interior as a result of the intrusions. An analytical model of the interior flow, which assumes a viscous-diffusive force balance and employs only molecular values of the transport coefficients, is found to be consistent with the experimental observations. The model, in agreement with the dye observations, predicts negligible vertical mass transport.

Since in the interior there is no measurable horizontal gradient of density, the gradual weakening of the vertical density gradient must therefore be due to vertical differential advection. This advective flow is necessarily part of slow cellular motions in which fluid exits horizontally from a vertical region adjacent to the grid, is advected vertically in the interior, and returns along the horizontal top and bottom boundaries to the region adjacent to the grid. It is surmised that these two cells are driven by a buoyancy layer near the grid. To understand the details of the evolution of the density gradient and of the circulation pattern requires further observations, particularly within the turbulent zone.

The vertical mass flux is a function of the grid-generated turbulence parameters and the mean density gradient in the turbulent region. Measurements of these parameters and of the mass flux indicate that the flux increases with the grid frequency of oscillation, the amplitude of oscillation, and the mean-density gradient (25).

The authors would like to thank Laurence Armi, Frederick Sherman, Jörg Imberger and Hugo Fischer, from whom we have derived substantial benefit in discussion of our work. This work, based on a Ph.D. thesis submitted to the University of California, Berkeley, by the first author, was undertaken while he was the recipient of a Gladden

Postgraduate Studentship from the University of Western Australia. Additional financial support was provided by the University of California Water Resources Center, as part of Water Resources Center Project UCAL-WRC-W-525.

## REFERENCES

- ARMI, L. 1978 Some evidence for boundary mixing in the deep ocean. *J. Geophys. Res.* **83**, 1971-1979.
- ARMI, L. 1979 Effects of variation in eddy diffusivity on property distributions in the ocean. *J. Mar. Res.* **37**, 515-530.
- ARMI, L. & D'ASARO, E. 1980 Flow structures of the benthic ocean. *J. Geophys. Res.* **85**, 469-484.
- ARMI, L. & MILLARD, R. C. 1976 The bottom boundary layer of the deep ocean. *J. Geophys. Res.* **81**, 4983-4990.
- CALDWELL, D. R., BRUBAKER, J. M. & NEAL, V. T. 1978 Thermal microstructure on a lake slope. *J. Limn. Oceanog.* **23**, 372-374.
- CHEN, C. F., BRIGGS, D. G. & WIRTZ, R. A. 1971 Stability of thermal convection in a salinity gradient due to lateral heating. *Int. J. Heat Mass Transfer* **14**, 57-65.
- FISCHER, H. B., LIST, E. J., KOH, R. C. Y., IMBERGER, J. & BROOKS, N. H. 1979 *Mixing in Inland and Coastal Waters*. Academic.
- FORTUIN, J. 1960 Theory and application of two supplementary methods of constructing density gradient columns. *J. Polymer Sci.* **44**, 505-515.
- GARRETT, C. 1979a Mixing in the ocean interior. *Dyn. Oceans Atmos.* **3**, 239-266.
- GARRETT, C. 1979b Comment on 'Some evidence for boundary mixing in the deep ocean' by L. Armi. *J. Geophys. Res.* **84**, 5095-5096.
- GREENSPAN, H. P. & HOWARD, L. N. 1963 On a time-dependent motion of a rotating fluid. *J. Fluid Mech.* **17**, 385-404.
- GREGG, M. C. & SANFORD, T. B. 1980 Signatures of mixing from the Bermuda slope, the Sargossa Sea and the Gulf Stream. *J. Phys. Oceanog.* **10**, 105-127.
- HOGG, N. G., KATZ, E. J. & SANFORD, T. B. 1978 Eddies, islands and mixing. *J. Geophys. Res.* **83**, 2921-2938.
- HOPFINGER, E. J. & TOLY, J. A. 1976 Spatially decaying turbulence and its relation to mixing across density interfaces. *J. Fluid Mech.* **78**, 155-175.
- IMBERGER, J., THOMPSON, R. T. & FANDRY, C. 1976 Selective withdrawal from a finite rectangular tank. *J. Fluid Mech.* **78**, 489-512.
- KRAUSS, E. B. (ed.) 1977 *Modelling and Prediction of the Upper Layers of the Ocean*. Pergamon.
- MANINS, P. C. 1976 Intrusion into a stratified fluid. *J. Fluid Mech.* **74**, 547-560.
- MAXWORTHY, T. 1972 Experimental and theoretical studies of horizontal jets in a stratified fluid. In *Proc. Int. Symp. on Stratified Flows, Novosibirsk*.
- MUNK, W. 1966 Abyssal recipes. *Deep-Sea Res.* **13**, 707-730.
- SHERMAN, F. S., IMBERGER, J. & CORCOS, G. M. 1978 Turbulence and mixing in stably stratified waters. *Ann. Rev. Fluid Mech.* **10**, 267-288.
- THORPE, S. A., HUTT, P. K. & SOULSBY, R. 1969 The effect of horizontal gradients on thermohaline convection. *J. Fluid Mech.* **38**, 375-400.
- TURNER, J. S. 1973 *Buoyancy Effects in Fluids*. Cambridge University Press.
- VERONIS, G. 1970 The analogy between rotating and stratified fluids. *Ann. Rev. Fluid Mech.* **2**, 37-66.
- WUNSCH, C. 1972 Temperature microstructure on the Bermuda Slope with application to the mean flow. *Tellus* **24**, 350-367.